

The Two Photocycles of Photoactive Yellow Protein from *Rhodobacter sphaeroides**

Received for publication, September 12, 2002, and in revised form, December 20, 2002
Published, JBC Papers in Press, December 20, 2002, DOI 10.1074/jbc.M209343200

Andrea Haker‡, Johnny Hendriks‡, Ivo H. M. van Stokkum§, Joachim Heberle¶, Klaas J. Hellingwerf‡, Wim Crielaard‡, and Thomas Gensch||**

From the ‡Laboratory for Microbiology, Swammerdam Institute for Life Sciences, BioCentrum, University of Amsterdam, Nieuwe Achtergracht 166, 1018 WV Amsterdam, The Netherlands, §Faculty of Sciences, Vrije Universiteit, De Boelelaan 1081, 1081 HV Amsterdam, The Netherlands, and ¶Institute of Biological Information Processing 2 (IBI-2) and ||Institute of Biological Information Processing 1 (IBI-1), Research Centre Jülich, D-52425 Jülich, Germany

The absorption spectrum of the photoactive yellow protein from *Rhodobacter sphaeroides* (R-PYP) shows two maxima, absorbing at 360 nm (R-PYP₃₆₀) and 446 nm (R-PYP₄₄₆), respectively. Both forms are photoactive and part of a temperature- and pH-dependent equilibrium (Haker, A., Hendriks, J., Gensch, T., Hellingwerf, K. J., and Crielaard, W. (2000) *FEBS Lett.* 486, 52–56). At 20 °C, for PYP characteristic, the 446-nm absorbance band displays a photocycle, in which the depletion of the 446-nm ground state absorption occurs in at least three phases, with time constants of <30 ns, 0.5 μ s, and 17 μ s. Intermediates with both blue- and red-shifted absorption maxima are transiently formed, before a blue-shifted intermediate (pB₃₆₀, λ_{\max} = 360 nm) is established. The photocycle is completed with a monophasic recovery of the ground state with a time constant of 2.5 ms. At 7 °C these photocycle transitions are slowed down 2- to 3-fold. Upon excitation of R-PYP₃₆₀ with a UV-flash (330 \pm 50 nm) a species with a difference absorption maximum at \sim 435 nm is observed that returns to R-PYP₃₆₀ on a minute time scale. Recovery can be accelerated by a blue light flash (450 nm). R-PYP₃₆₀ and R-PYP₄₄₆ differ in their overall protein conformation, as well as in the isomerization and protonation state of the chromophore, as determined with the fluorescent polarity probe Nile Red and Fourier Transform Infrared spectroscopy, respectively.

Photoactive yellow protein (PYP)¹ is a photoreceptor that has been found in several purple bacteria (1). The first, and so far best studied example for this group of blue light receptors, was found in *Ectothiorhodospira halophila* (E-PYP) (2). The chromophore, responsible for the photophysical properties of PYP, is 4-hydroxy-cinnamic acid that is bound to Cys-69 via a thioester linkage (3, 4). The crystal structure of this small protein, consisting of 125 amino acids, has been solved to 1.4-Å resolution (5) and shows an α/β -fold, which has become the prototype

for the folding of the Per-Arnt-Sim domain superfamily (6, 7). In the ground state the chromophore is deprotonated and buried in a hydrophobic pocket of the protein where its negative charge is stabilized via a hydrogen bonding network. Absorption of light induces a photocycle in E-PYP, in which isomerization of the chromophore is the initial step, which leads to the formation of several transient intermediates on the femtosecond to nanosecond timescale (8, 9). Within a few nanoseconds an intermediate is formed (pR₄₆₅, also named I₁ or PYP_L; λ_{\max} = 465 nm) and red-shifted with respect to the ground state absorption maximum (λ_{\max} = 446 nm). pR₄₆₅ decays into a blue-shifted intermediate (pB₃₅₅, also named I₂ or PYP_M; λ_{\max} = 355 nm) with time constants of 200 μ s and 1.2 ms (10, 11). This latter transition is accompanied by protonation of the phenolic oxygen of the chromophore and by subsequent conformational changes of the protein (12, 13). It is suggested that pB₃₅₅ is the signaling state of PYP. From pB₃₅₅ the ground state pG₄₄₆ is recovered in a biexponential process with time constants of 200 ms and \sim 1 s (11). The pR₄₆₅ to pB₃₅₅ and pB₃₅₅ to pG₄₄₆ transitions are very sensitive to both temperature and pH (14, 15).

In contrast to the detailed knowledge available for PYP from *E. halophila*, other photoactive yellow proteins are biophysically poorly investigated. So far, proteins from three other species were purified and basically characterized: (i) PYP from *Rhodospirillum rubrum* (16), which shares 71% amino acid sequence identity with E-PYP and has virtually the same ground state absorption spectrum (λ_{\max} = 445 nm) and similar kinetics of photobleaching and recovery (with time constants for pB formation and pG recovery of 85 μ s and 210 ms, respectively); (ii) PYP-phytochrome-related protein from *Rhodospirillum rubrum* (17), a hybrid-protein, consisting of 884 amino acids, with an N-terminal PYP domain fused to a central phytochrome-like domain and a C-terminal histidine kinase domain. When heterologously expressed and reconstituted with 4-hydroxy-cinnamic acid, Ppr displays an absorbance maximum at 434 nm and is photoactive; bleaching at 434 nm is accompanied by the initial formation of a red-shifted intermediate with a difference absorption maximum at \sim 470 nm, and subsequently a blue-shifted intermediate is formed with a difference absorption maximum at \sim 330 nm. The recovery to the ground state is biphasic with a fast and a very slow component (lifetimes of 0.21 ms and 46 s, respectively); and (iii) PYP from *Rhodobacter sphaeroides* (R-PYP), which has been characterized in some more detail (18) and is also the subject of this study.

Heterologously expressed R-PYP, reconstituted *in vitro* with 4-hydroxy-cinnamic acid, is a yellow-colored and photoactive protein (18). The main absorption band with a maximum at 446

* The costs of publication of this article were defrayed in part by the payment of page charges. This article must therefore be hereby marked "advertisement" in accordance with 18 U.S.C. Section 1734 solely to indicate this fact.

** Recipient of a Casimir-Ziegler fellowship from the Royal Dutch Academy of Sciences and The Academy of Sciences of Nordrhein-Westfalen. To whom correspondence should be addressed. Tel.: 49-02461-618068; Fax: 49-02461-614216; E-mail: t.gensch@fz-juelich.de.

¹ The abbreviations used are: PYP, photoactive yellow protein; E-PYP, PYP from *Ectothiorhodospira halophila*; R-PYP, PYP from *Rhodobacter sphaeroides*; SAS, species-associated spectrum, CCD, charged-coupled device; FT-IR, Fourier Transform Infrared; NR, Nile Red.

nm (R-PYP₄₄₆) can be reversibly bleached by irradiation with blue light, which leads to the formation of a blue-shifted intermediate with a difference absorption maximum at 360 nm (formerly designated as pB₃₅₀; because of our new results presented in this paper it is now named pB₃₆₀). pB₃₆₀ of R-PYP relaxes to the ground state of R-PYP₄₄₆, pG₄₄₆, with a time constant of 2 ms. This recovery process is ~100-fold faster than in E-PYP and ~23,000-fold faster than in Ppr.

Moreover, the UV-visible absorption spectrum of R-PYP shows an additional peak, positioned at 360 nm, named R-PYP₃₆₀. R-PYP₃₆₀ and R-PYP₄₄₆ are jointly part of a temperature- and pH-dependent equilibrium. R-PYP₃₆₀ and R-PYP₄₄₆ can be reversibly interconverted by increasing/decreasing the temperature. Lowering the temperature leads to accumulation of R-PYP₃₆₀. Titration of the ground state of R-PYP in the pH range from 1.5 to 9 revealed two separate transitions, with pK_a values of 3.8 and 6.5 (18). Below pH 9 the absorbance at 446 nm decreases, whereas the absorbance at 360 nm increases at lower pH. Below pH 5, yet another spectral intermediate is formed, with a clearly further blue-shifted absorbance maximum (345 nm). This form is probably analogous to pB_{dark} of E-PYP, which is a partially unfolded protein state, formed at low pH (pK_a = 2.7) (19).

In the present study we extend our analysis of the photoactive properties of R-PYP. To gain a deeper insight into the photocycle of R-PYP₄₄₆ we measured laser-induced transient absorption changes, with high spectral (charged-coupled device (CCD) camera) and temporal (photomultiplier) resolution at two different temperatures. Measurements were complicated by the light sensitivity of R-PYP₃₆₀, which also undergoes a photocycle after absorption of light. In addition, the protein conformation of the two forms of R-PYP was examined with respect to accessible hydrophobic surface areas, using the fluorescent polarity probe Nile Red. The isomerization and protonation state of the chromophore and some features of the hydrogen bonding network for both ground state species of R-PYP and their longest living photocycle intermediates were studied by FT-IR spectroscopy.

MATERIALS AND METHODS

Sample Preparation—R-PYP was heterologously overexpressed in *Escherichia coli* and purified as described earlier (18). Apo-R-PYP was reconstituted using activated 4-hydroxy-cinnamic acid as described previously (14) or 7-hydroxy-coumarin-3-carboxylic acid (referred to as locked chromophore) as in Ref. 20. E-PYP was produced and purified as described (1). Samples were analyzed in 50 or 100 mM Tris-HCl buffer at pH 7.5 to 8.

Steady State and Transient UV-visible Measurements—Steady state absorption spectra of R-PYP were measured on a HP 8453 UV-visible diode array spectrophotometer (Hewlett-Packard Nederland BV, Amstelveen, The Netherlands). The photocycle of R-PYP₃₆₀ was also investigated on this spectrophotometer using variable time resolutions ranging from 1 to 300 s. R-PYP₃₆₀ was excited using a photo flashlight (500-μs pulse width) equipped with a 330 ± 50-nm band-pass filter. To examine spectral changes after a subsequent blue flash, the same set-up was used but with a 450 ± 7-nm interference filter.

Laser-flash Photolysis Spectroscopy—The photocycle of R-PYP₄₄₆ was studied using an Edinburgh Instruments Ltd. LP900 spectrometer (Livingston, West Lothian, United Kingdom), equipped with both a CCD camera and a photomultiplier, in combination with a Continuum Surelite optical parametric oscillator laser (for further details see Ref. 21). The sample was excited with 465-nm laser flashes of 6 to 9 mJ (pulse width 6 ns). In a number of experiments, a 400-nm long-pass or a 450 ± 7-nm interference filter was introduced into the observation light beam, before the sample, to reduce secondary photochemistry. The probe light intensity was maximally reduced, while maintaining an acceptable signal/noise ratio. Time-gated spectra were recorded using the CCD camera, averaging 10 to 50 single measurements. Time traces were measured at different wavelengths between 400 and 500 nm, using the photomultiplier. Data of 64 recordings were averaged for each trace.

The measurements were carried out at 20 ± 1 or 7 ± 2 °C in a water-cooled sample cell. The temperature was regularly monitored directly in the sample. For experiments at 7 °C the sample chamber was flushed with nitrogen gas to prevent condense formation. Data were globally fitted by multiexponential functions using nonlinear least-square procedures from the Microcal Origin software package or with the help of a home-developed global and target analysis package described elsewhere (22, 23).

Fluorescence Experiments—Fluorescence was measured in a 1-cm cuvette using an AMINCO Bowman Series 2 luminescence spectrometer (Thermo Spectronic, Rochester, NY). For determination of the emission spectra of the two spectral species of R-PYP, the excitation wavelengths were 446 and 360 nm (bandwidth, 16 nm), and emission was recorded at a rate of 1 nm/s from 450 to 600 nm and from 365 to 600 nm (bandwidth, 4 nm), respectively. Fluorescence excitation spectra were detected from 300 to 490 nm and 300 to 430 nm (bandwidth, 16 nm) by measuring the emission at 496 and 440 nm (bandwidth, 4 nm), respectively. The fluorescence quantum yield for the 446-nm spectral form of R-PYP in 50 mM Tris-HCl, pH 8, was determined by comparing its fluorescence with that of E-PYP (Φ_F = 0.002) (24). Both samples were excited at 446 nm with equal absorption at this wavelength.

Nile Red Binding Assay—For the Nile Red binding studies, 20 μl of a 100 μM Nile Red stock solution (in dimethyl sulfoxide) was added to a 1980-μl sample of R-PYP or locked R-PYP (R-PYP reconstituted with the locked chromophore) with an A₄₄₆ of 0.1. Measurements were started 30 s after the addition of the probe. The emission spectrum was recorded from 555 to 800 nm (bandwidth, 4 nm) with excitation at 540 nm (bandwidth, 16 nm). The measurements were carried out at room temperature (~20 °C) or at ~12 °C. The cuvette was water-cooled; the temperature was monitored in the cuvette.

FT-IR Spectroscopy—FT-IR difference spectroscopy was performed on a Bruker IFS 66v spectrometer. Spectral resolution was set to 2 cm⁻¹ in the photoconversion experiments and 4.5 cm⁻¹ in the low temperature experiments. In the conventional transmission technique, used for the photoconversion experiments, a droplet of a highly concentrated sample solution was put on a BaF₂ cuvette and sealed by a cover window of the same material (see Ref. 25 for more experimental details). For light excitation either the 3rd harmonic of a Nd:YAG laser (Quanta Ray GRC 12S) was used (20 pulses of 8-ns duration and 20 mJ of energy at 355 nm each), or this laser light was fed into a tunable optical parametric oscillator to produce 100 pulses of 5-ns duration each and 2 mJ of energy at 445 nm. Laser emission was guided to the sample through a quartz fiber bundle to achieve homogenous illumination.

Low temperature, blue light-induced, FT-IR difference spectroscopy was performed using the attenuated total reflection technique. An attenuated total reflection accessory was used with a diamond disc as the internal reflection element (26). 10 μl of the protein solution was put on the diamond surface and concentrated by a stream of nitrogen. Rehydration by 2 μl of water resulted in a 2:1 ratio of the band heights around 1650 cm⁻¹ (amide I overlapped by H₂O bending mode) and 1550 cm⁻¹ (amide II), which demonstrates good hydration of the protein. Blue light illumination was done via a cold light source equipped with a fiber bundle (Schott, Mainz, Germany). In all light-induced difference experiments, a broadband interference filter (OCLI) was inserted in front of the mercury-cadmium-telluride detector to protect it from stray light and to limit the spectral range to 1850 to 950 cm⁻¹. The temperature of the sample was controlled by a circulating water bath filled with ethanol.

RESULTS

Fluorescence Spectra of R-PYP—The absorption spectrum of R-PYP is characterized by the presence of an equilibrium between two species with maxima at 360 and 446 nm, respectively. The fluorescence emission and excitation spectra of these species are shown in Fig. 1. Excitation at 446 nm yielded an emission spectrum with a maximum at 496 nm. Excitation at 360 nm resulted in additional fluorescence at ~440 nm. The fluorescence quantum yield of R-PYP₄₄₆ was calculated as 0.03 (see "Materials and Methods"). The corresponding fluorescence excitation spectra (Fig. 1), recorded at 440 and 496 nm, yielded maxima at 360 and 446 nm, respectively, representing the two forms, R-PYP₃₆₀ and R-PYP₄₄₆, as also observed in the absorption spectrum.

Photocycle of R-PYP₄₄₆—The ability to undergo a photocycle after light absorption is a characteristic feature of all known

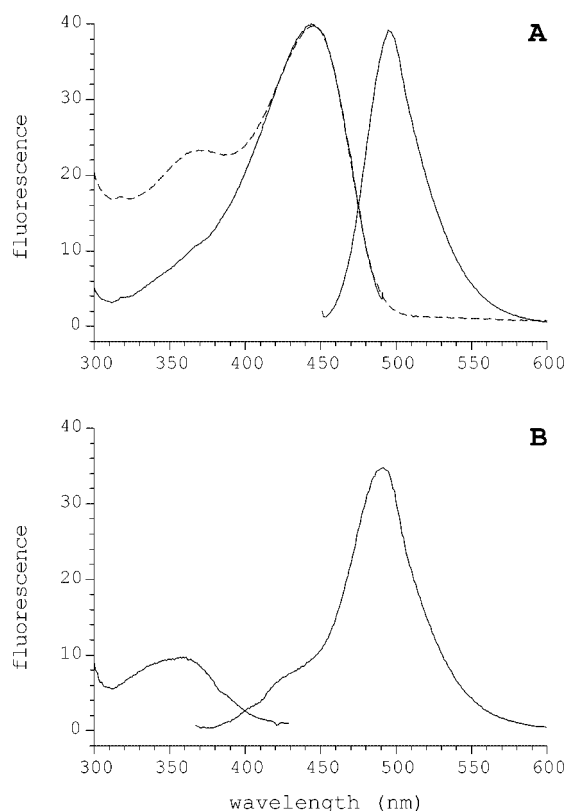


FIG. 1. Fluorescence emission and excitation spectra of R-PYP. A, emission spectrum with excitation at 446 nm and excitation spectrum monitored at 496 nm are plotted. The dashed line represents the absorption spectrum of R-PYP (adapted to scale for convenience). B, emission spectrum with excitation at 360 nm and excitation spectrum monitored at 440 nm are plotted.

PYPs. Also the yellow form of R-PYP, R-PYP₄₄₆, displays such a photocycle. Absorption difference spectra recorded after excitation with a 465-nm laser flash are shown in Fig. 2. After 30 ns, positive absorption changes at 380 nm and at 480 nm are visible, together with a large negative signal at 446 nm reflecting the bleach of the ground state. At the next time point (500 ns) the positive red-shifted absorption, with respect to the ground state absorption maximum at 446 nm, has decreased, whereas the blue-shifted absorption has shifted toward 355 nm. In the following phase the blue-shifted absorption increases, accompanied by a further decrease in the absorption at 446 nm. These processes are completed at 60 μ s (Fig. 2A). The recovery phase of the photocycle is shown in Fig. 2B, where the blue-shifted intermediate is returning into the ground state pG₄₄₆ within 10 ms. This recovery seems to be incomplete. We attribute this finding (a residual absorption difference) to secondary photochemical processes induced by the observation light (see below).

Photocycle of R-PYP₃₆₀—In addition to R-PYP₄₄₆, R-PYP₃₆₀ can also be bleached by light. Fig. 3A shows an absorption difference spectrum of R-PYP after illumination with UV light. The bleach of R-PYP₃₆₀ is accompanied by an increase in absorption at \sim 435 nm; we have named this latter state R-PYP₄₃₅. This transformation occurs within a time shorter than 100 ms. A subsequent 450-nm light flash induces the recovery of R-PYP₃₆₀ (not shown), again faster than 100 ms. Both phototransformations could not be studied at higher time resolution because of photochemistry induced by the observation light. Obviously this effect is getting more pronounced at higher probe light intensities, obligatory for nanosecond to millisecond flash photolysis experiments. R-PYP₄₃₅ returns back to R-PYP₃₆₀ in the dark on a minute time scale (see Fig.

3B). Determination of a more accurate time constant again is not possible (in our set-up) because of the extreme light sensitivity of R-PYP₄₃₅.

This second photocycle of R-PYP also explains the residual absorption difference in the laser excitation (465 nm) photocycle measurements (see Fig. 2B). The observation light below 400 nm photoactivates R-PYP₃₆₀ and, as a result, leads to accumulation of the R-PYP₄₃₅ intermediate (with a minute lifetime). Subsequently, 465-nm laser light induces, in addition to the intended photoactivation of R-PYP₄₄₆, the light-driven recovery of R-PYP₄₃₅ to R-PYP₃₆₀. A photoequilibrium of R-PYP₃₆₀ (excited continuously during the 100-ms measurement cycle by the observation light) and R-PYP₄₃₅ (photoconverted within 6 ns by the blue excitation laser) is then established, which is reflected in a residual absorption difference (see e.g. the 10-ms absorption difference spectrum in Fig. 2B).

To determine the influence of this secondary photochemistry on the characteristics of the R-PYP₄₄₆ photocycle we performed laser flash photolysis experiments while using a 450 ± 7 -nm band-pass filter placed into the observation light beam. Fig. 4A shows kinetic traces recorded at 450 nm after excitation with a 465-nm laser flash. The bleach at 446 nm occurs biexponentially with time constants of 0.5 and 17 μ s (see Table I). The recovery of the ground state can be fitted monoexponentially with a time constant of 2.8 ms. Time constants determined in the absence or presence of the filter in the observation light path are virtually identical (see Table I). Recovery, however, is completed to zero when using the 450-nm filter and to a negative value, reflecting R-PYP₄₃₅ transformed to R-PYP₃₆₀, without the filter (Fig. 4B).

The R-PYP₄₄₆ Photocycle at Two Different Temperatures—To examine whether the formation of the different intermediates is temperature-sensitive, we studied the R-PYP₄₄₆ photocycle at two different temperatures (20 and 7 $^{\circ}$ C). A 400-nm long-pass filter in the observation light beam was used to prevent secondary photochemistry (see above). The entire photocycle is slowed down 2- to 3-fold at 7 $^{\circ}$ C (see Table I). Fig. 5 shows the calculated decay-associated difference spectra from the data obtained in the time-resolved CCD measurements, for both temperatures. At 7 $^{\circ}$ C the shape and relative amplitude of the first decay-associated difference spectra compared with the second are distinctly different from the situation at 20 $^{\circ}$ C. At low temperature the intermediate(s) absorption decay in the range of 400 to 440 nm is much more associated with the first component. The varying shape and relative amplitude of the decay-associated difference spectra indicate that indeed a mixture of intermediates is formed during the photocycle, of which the relative amounts vary in a temperature-dependent way.

Time-resolved spectra analogous to those shown in Fig. 2 were subjected to global target analysis using a sequential model with three components, and the fluorescence excitation spectrum were obtained with detection at 496 nm (see Fig. 1) as the ground state spectrum pG₄₄₆ of R-PYP₄₄₆. To be able to include information on the absorption changes below 400 nm, we generated data in time-gated measurements without the placement of a filter in the observation light beam. The estimated species-associated spectra of the three components at 20 $^{\circ}$ C are shown in Fig. 6A. Clearly, the 3rd component (dashed) resembles the typical blue-shifted intermediate pB, known from E-PYP and Ppr, with a maximum at 360 nm (pB₃₆₀, formerly designated as pB₃₅₀) (18). The spectra of the first two components are very broad, and the second is also very structured. They presumably both represent a mixture of several intermediates, including a species analogous to pR₄₆₅ from E-PYP, but obviously there is also at least one with a blue-shifted absorption maximum (with respect to R-PYP₄₄₆).

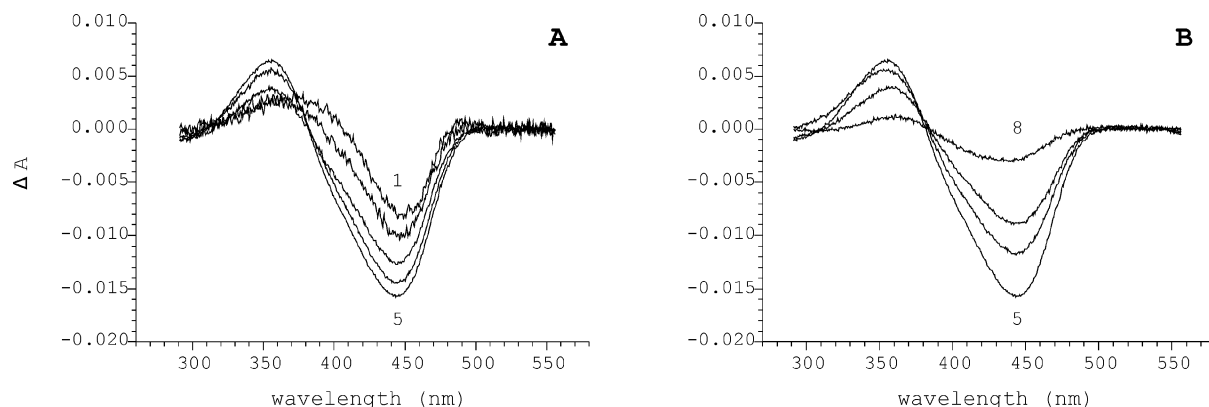


FIG. 2. Time resolved difference absorption spectra of R-PYP at 20 °C after 465-nm laser excitation. Spectra 1 to 8 are taken after 30 ns, 500 ns, 5 μ s, 15 μ s, 60 μ s, 500 μ s, 1 ms, and 10 ms, respectively.

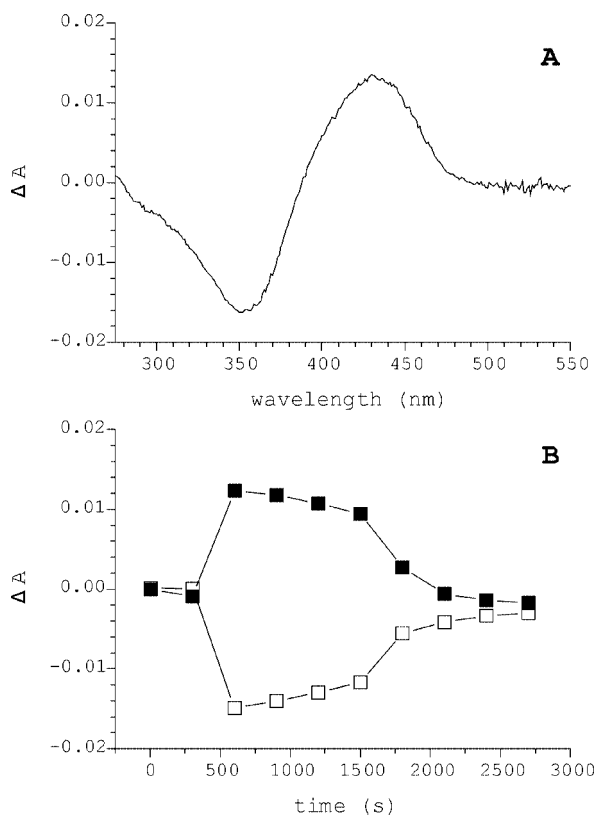


FIG. 3. The photocycle of R-PYP₃₆₀. A, absorption difference spectrum of R-PYP after a UV flash (330 \pm 50 nm). B, time course of the absorption at 440 nm (filled symbols) and 360 nm (open symbols) after a UV flash (applied at the 500-s time point).

The estimated species-associated spectra for the photocycle at 7 °C, presented in Fig. 6B, again show the formation of a blue-shifted pB₃₆₀ intermediate (dashed), now with some additional absorption at about 410 nm, compared with the spectra measured at 20 °C. Moreover, again the first and second species-associated spectra are very broad, the latter showing again sub-structures, but with less absorption at around 410 nm and a more pronounced contribution at 465 nm. Comparison of the species-associated spectra obtained at both temperatures clearly shows the presence of several components prior to the formation of pB₃₆₀ in the R-PYP₄₄₆ photocycle. We performed a global fit for these data to resolve the spectra of the involved species (shown also in Fig. 6). For the first two intermediates the presence of three species with absorption maxima at 360, 415, and 465 nm (pB'₃₆₀, pB'₄₁₅, and pR₄₆₅, respectively) can be fitted reasonably well. The relative contributions do vary with

temperature (see legend of Fig. 6). Subsequently, pB₃₆₀ is accumulated with, at 7 °C, a contribution of the 415 species.

Nile Red Bindings Assays—In R-PYP we have found the special situation for PYP that both species visible in the absorption spectrum are photoactive. To examine the nature of these two forms we have performed Nile Red (NR) binding assays. NR can be used as a fluorescent probe to obtain information about the accessible hydrophobic surface area of a protein. The fluorescence of NR in a hydrophilic environment (here aqueous buffer) is very low and has a maximum at 660 nm (Fig. 7). When R-PYP is added, the fluorescence increases and shifts toward shorter wavelengths ($\lambda_{\text{max}} = \sim 620$ nm), reflecting the binding of NR to a hydrophobic surface (12). In contrast, the binding of NR to R-PYP reconstituted with a locked chromophore (displaying a single absorption band at 441 nm) (18) is very low, and the fluorescence maximum is only slightly blue-shifted ($\lambda_{\text{max}} = \sim 657$ nm). Presumably, R-PYP₃₆₀ is primarily responsible for binding of NR because of the exposure of a hydrophobic region. This finding is supported by the change in fluorescence (both in amplitude (increased) and position (blue-shifted) of the maximum) at lower temperatures, where because of the thermal equilibrium between R-PYP₃₆₀ and R-PYP₄₄₆, a transition takes place from R-PYP₄₄₆ to R-PYP₃₆₀ (18). The change in the NR emission is reversible as expected for a thermal equilibrium (results not shown).

Another possibility to drive the equilibrium more toward R-PYP₃₆₀ is a decrease of the pH. As can be seen from Fig. 7, a change to pH 5 increases the fluorescence dramatically, demonstrating again the presence of an exposed hydrophobic region. The maximum of the fluorescence emission is red-shifted ($\lambda_{\text{max}} = \sim 640$ nm) compared with R-PYP at pH 8, indicating a change in the characteristics of the Nile Red binding site, possibly because of protonation of an amino acid in or near the Nile Red binding site.

FT-IR Spectroscopy—The main focus of the FT-IR spectroscopic experiments was the determination of the protonation and isomerization state of the chromophore in both ground state forms of R-PYP. The long lifetime of R-PYP₄₃₅ allowed us to accumulate R-PYP₄₃₅ by excitation with 355 nm of light. The corresponding FT-IR difference spectrum (R-PYP₄₃₅–R-PYP₃₆₀) is shown in Fig. 8 (trace 1). R-PYP₄₃₅ could be illuminated back to R-PYP₃₆₀ by using 445 nm of laser light. In the corresponding difference spectrum (Fig. 8A, trace 3) all the major bands appear with a reverted sign. This illumination back and forth was reproducible with high accuracy. Trace 2 shows the sum of the two difference spectra (corrected for the difference in the extent of photoconversion because of our experimental conditions) demonstrating the reversibility. The high noise in trace 2 in some regions (*i.e.* in the ranges from 1695 to 1570 cm^{-1} and

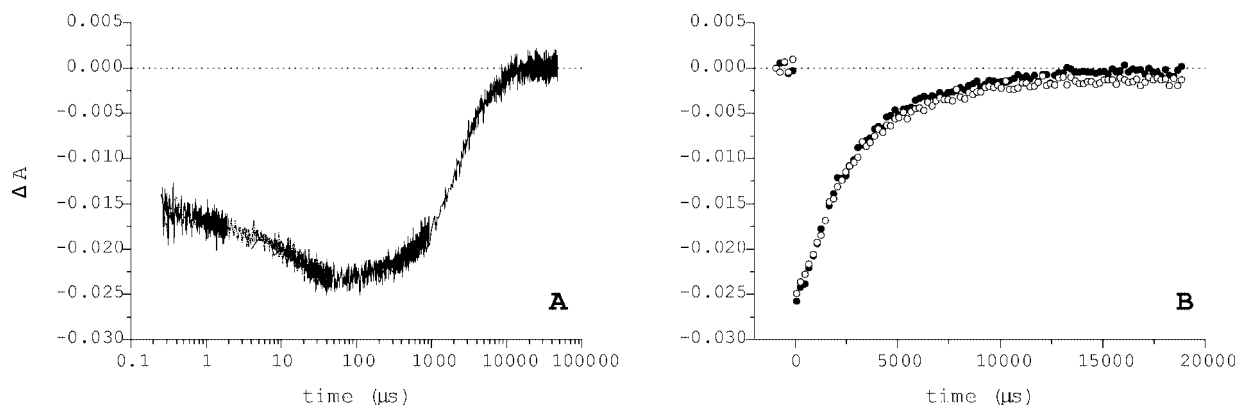


FIG. 4. Kinetic traces of absorbance changes at 450 nm after 465-nm laser excitation at 20 °C. **A**, traces were measured in four different time windows. A 450 ± 7 -nm interference filter was introduced in the observation light beam. **B**, traces were measured in a time window up to 20 ms. No filter (open circles) or a 450-nm interference filter (filled circles) was introduced in the observation light. Each data point represents the average of five time points.

TABLE I

Time constants measured for the R-PYP₄₄₆ photocycle

Measurements of kinetic traces at 450 nm were carried out with or without a 450 ± 7 -nm interference filter in the observation light beam at 20 °C (upper part). Data for measurements at both temperatures were determined from time-resolved measurements combining the analysis of time-gated spectra and time-traces (lower part). Traces were globally fitted for all measured wavelengths from 400 to 500 nm with two components for the bleach and one component for the recovery of the 446-nm form. The data from the recorded spectra were averaged over 9 nm, and a tri-exponential global fit was performed over all wavelengths and time points.

Traces 450 nm	τ_1	τ_2	τ_3
With filter	$0.5 \pm 0.25 \mu\text{s}$	$17 \pm 3 \mu\text{s}$	$2.8 \pm 0.2 \text{ ms}$
Without filter	$0.6 \pm 0.25 \mu\text{s}$	$18 \pm 3 \mu\text{s}$	$2.9 \pm 0.2 \text{ ms}$
T-dependent τ 's			
20 °C	$0.5 \pm 0.15 \mu\text{s}$	$16 \pm 2 \mu\text{s}$	$2.5 \pm 0.4 \text{ ms}$
7 °C	$1.1 \pm 0.25 \mu\text{s}$	$40 \pm 4 \mu\text{s}$	$8.0 \pm 0.7 \text{ ms}$
$\tau_1(7^\circ\text{C})/\tau_1(20^\circ\text{C})$	2.2	2.5	3.2

1120 to 980 cm^{-1}) because of strong absorption of the sample indicates that accuracy of band positions and amplitudes of the difference spectra will be low in these regions.

A first inspection of the R-PYP₄₃₅-R-PYP₃₆₀ difference spectrum (Fig. 8A, trace 1) shows a number of bands known (and partially assigned) from FT-IR studies on E-PYP (e.g. the positive bands at 1627, 1489 (with a shoulder at 1504), 1304, and 1158 cm^{-1} and the negative bands 1645, 1516, 1287, and 1170 cm^{-1}). Some other large features (e.g. at 1145 and 993 cm^{-1}), however, are new or very different in their intensity. Interestingly, no change is observed above 1700 cm^{-1} indicating no change in the Glu-46 protonation state and the hydrogen bonding strength of its deprotonated carboxyl group.

R-PYP₃₆₀ and R-PYP₄₃₅ have no analogues among the known intermediate states in E-PYP, though the chromophore and its binding position are identical, and many important amino acids (e.g. Glu-46, Tyr-42, Arg-52) are conserved in R-PYP. To use the assignment of vibrational modes in E-PYP to characterize four R-PYP states (R-PYP₄₄₆, pB₃₆₀, R-PYP₃₆₀, R-PYP₄₃₅) we decided to measure a second difference spectrum, namely pB₃₆₀-R-PYP₄₄₆. When irradiating a concentrated R-PYP sample at -20°C with blue light (445 nm) a photocycle intermediate was accumulated, owing a lifetime of minutes, that showed a FT-IR difference spectrum similar to pB₃₅₅-pG₄₄₆ of E-PYP (see Fig. 8B, traces 4 and 5, and see Table II). We tentatively identify this accumulated intermediate as the photocycle inter-

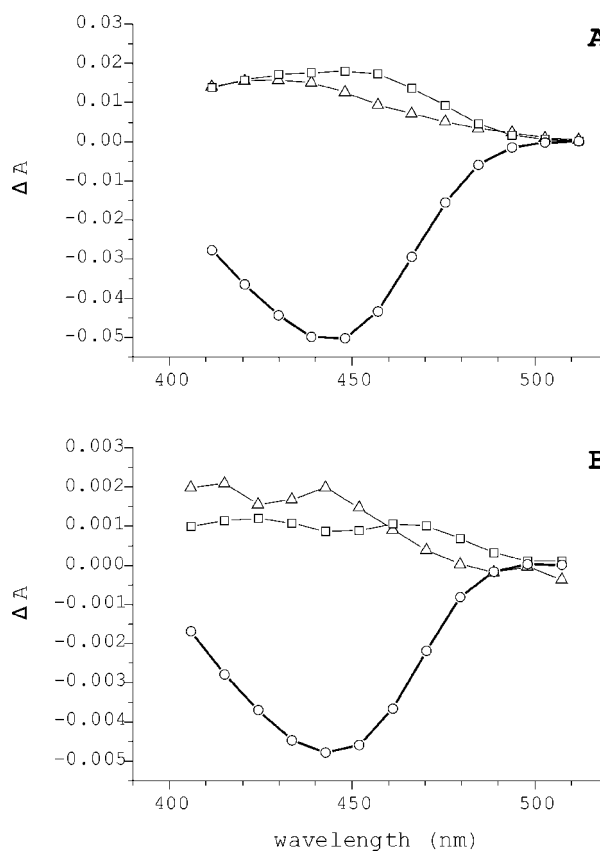


FIG. 5. Decay associated difference spectra of the R-PYP₄₄₆ photocycle. CCD spectra were measured at 20 °C (**A**) and 7 °C (**B**) with a 400-nm long-pass filter placed in the observation light beam. Difference spectra were averaged over 9 nm, and data were globally fitted with a triexponential function. The amplitude for the first (triangles), second (squares), and third (circles) component was plotted.

mediate pB₃₆₀ from R-PYP₄₄₆. For the discussion of the state of chromophore protonation and isomerization, with the help of assignments obtained in E-PYP, we consider only bands observed in both difference spectra of R-PYP to exclude false assignments of features caused by the different amino acid composition and/or different protein conformation of R-PYP with respect to E-PYP (see Table II). For comparison we also include a FT-IR difference spectrum pB₃₅₅-E-PYP₄₄₆ (see Fig. 8B, trace 5, and see Table II). This is very similar to previously published ones (13, 27, 28) except for the smaller change in the amide I region because of the relatively low hydration level of the sample used (29).

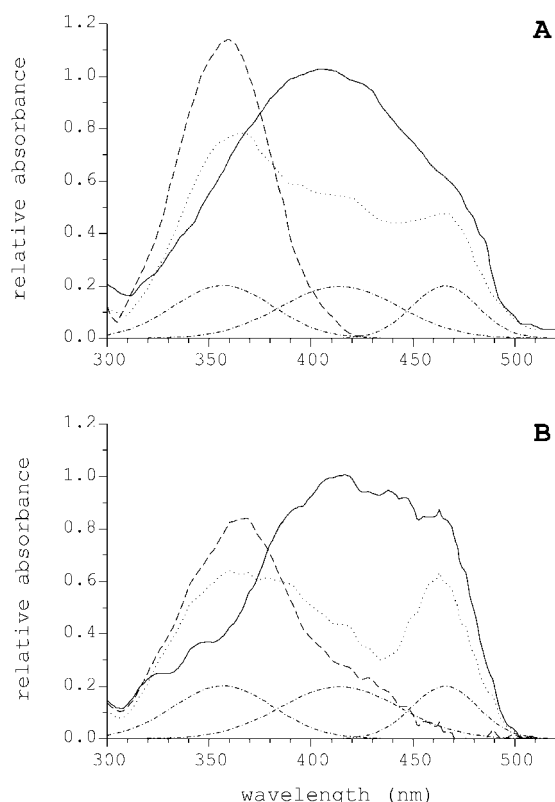


FIG. 6. Species-associated spectra (SAS) of the R-PYP₄₄₆ photocycle at 20 °C (A) and 7 °C (B). Spectra for three photocycle components were calculated from global target analysis of time-resolved difference spectra after a 465-nm laser flash. The estimated spectra of the first (solid line), second (dotted line), and third (dashed line) component are shown. Subsequently, the spectra of the first two components at both temperatures were globally fitted to a sum of three gaussian functions (with maxima at 358, 414, and 466 nm and standard deviations of 25, 29, and 16 nm, respectively) to resolve the spectra of the presumed species (dashed-dotted line). The relative amplitudes (i.e. the product of concentration and extinction coefficient) of the three spectra, pB₃₆₀, pB₄₁₅, and pR₄₆₅, are calculated as 27, 59, and 14% (1st SAS, 20 °C), 45, 38, and 17% (2nd SAS, 20 °C), 100, 0, and 0% (3rd SAS, 20 °C), 17, 62, and 21% (1st SAS, 7 °C), 45, 33, and 22% (2nd SAS, 7 °C), and 73, 17, and 0% (3rd SAS, 7 °C).

A pair of bands around 1500 cm⁻¹ (the band assigned to the PYP ground state will be given first from now on), 1498/1515 cm⁻¹ in D₂O (13) corresponding to 1485/1515 cm⁻¹ in H₂O (27, 28), is attributed to the phenolic ring vibration of the chromophore (13) and reflects the protonation state of the chromophore (with the 1515-cm⁻¹ band for the protonated chromophore). Two spectral features have been assigned to report about the isomerization state of the chromophore, namely 1302/1286 cm⁻¹ and 1163/~1175 cm⁻¹ (27, 28). A change in the hydrogen bonding of the carboxyl group of Glu-46 can be monitored from the band at 1737 cm⁻¹ (1727 cm⁻¹ in D₂O) assigned to the C = O stretching mode of Glu-46 (30).

By comparing the three difference spectra in Fig. 8B, it is obvious that there are large similarities between pB₃₅₅-E-PYP₃₄₆ and pB₃₆₀-R-PYP₄₄₆, especially at the spectral features assigned to the protonation and isomerization state of the chromophore. In contrast, R-PYP₃₆₀-R-PYP₄₃₅ shows similar bands but reverted signs. Careful analysis allows us to determine the protonation and isomerization state of the four R-PYP species (R-PYP₄₄₆, pB₃₆₀, R-PYP₃₆₀, R-PYP₄₃₅; see "Discussion").

DISCUSSION

Fluorescence—Fluorescence excitation and emission spectra were determined for both spectral species of R-PYP. Whereas

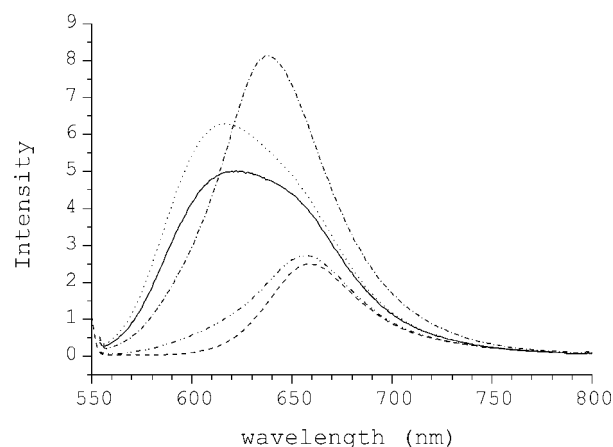


FIG. 7. Temperature-, pH-, and chromophore-type dependence of Nile Red binding to R-PYP. From a 100 μM Nile Red stock solution, 20 μl were added to 1980 μl of sample and mixed immediately by inverting. A fluorescence emission spectrum with excitation at 540 nm was recorded 30 s after addition of NR. Spectra are shown for NR added to R-PYP at 20 °C, pH 8 (solid line), 12 °C, pH 8 (dotted line), 20 °C, pH 5 (dashed-dotted line), to locked R-PYP at 20 °C, pH 8 (dashed-dot-dot line), and to the buffer at 20 °C, pH 8 (dashed line).

R-PYP₄₄₆ shows a maximum in emission at 496 nm, excitation at 360 nm reveals an additional fluorescence band centered at 440 nm, reflecting excitation of R-PYP₃₆₀. The Stokes shifts for the emission of R-PYP₃₆₀ and R-PYP₄₄₆ are 5051 and 2260 cm⁻¹, respectively. The fluorescence quantum yield (Φ_f) for the excitation at 360 nm is much lower than for excitation at 446 nm (Φ_{f-446}).

The fluorescence emission spectrum of R-PYP₄₄₆ is very similar to that of E-PYP; the maximum of the latter is only slightly blue-shifted (by 1 nm). Nevertheless, the fluorescence quantum yield for excitation at 446 nm is increased by about an order of magnitude in R-PYP (0.03 versus 0.002) (24). Interestingly, the Y42F mutant E-PYP also shows a highly increased Φ_f of 0.018 (31). This mutant protein displays also two maxima in the visible part of the ground state absorption spectrum (391 and 458 nm). However, the shape of the emission spectrum for excitation at both absorption maxima remains the same (31), whereas for R-PYP the excitation at 360 nm gives rise to a clearly different additional emission at ~440 nm. Excitation spectra recorded at either 440 or 496 nm clearly display the two species R-PYP₃₆₀ and R-PYP₄₄₆.

R-PYP₄₄₆ Photocycle—The ability of R-PYP to undergo a photocycle has been described earlier (18). In this study we have extended our analyses of the R-PYP₄₄₆ photocycle to a broader time range starting from 30 ns up to 20 ms, when the photocycle is completed. The analysis of time traces measured at a single wavelength (e.g. at 450 nm; see Fig. 4) yields three photocycle phases. The bleach of the ground state absorption at 20 °C can be fitted biexponentially with time constants of 0.5 and 17 μs (1.1 and 40 μs at 7 °C), whereas the recovery occurs monoexponentially with a time constant of 2.5 ms (8 ms at 7 °C). Although the examination of the R-PYP₄₄₆ photocycle was complicated by secondary photochemical events, through absorption of light by R-PYP₃₆₀, we were able to show that the two photocycles do not influence each other. Suppressing the R-PYP₃₆₀ photocycle by placing a filter in the observation light beam did not change the time constants for the R-PYP₄₄₆ photocycle (see Table I). Global target analysis of time-gated spectra using a three component sequential model reveals a quite complex photocycle scheme.

The species-associated spectra (see Fig. 6) for the first two components at both measured temperatures are very broad and structured; they possibly represent a mixture of different in-

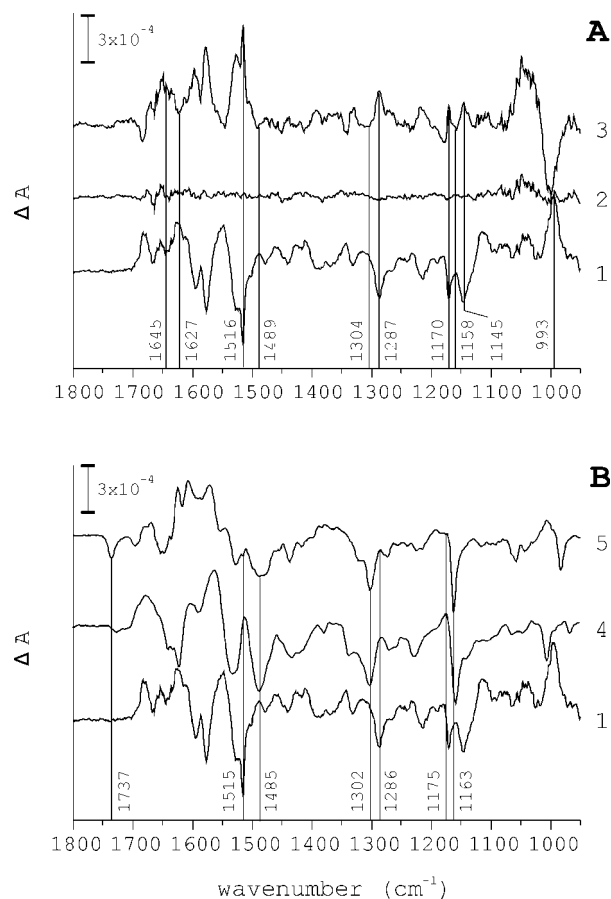


FIG. 8. **FT-IR difference spectra.** A, reversibility of R-PYP₃₆₀-R-PYP₄₃₅ infrared absorption: FT-IR absorption difference spectra R-PYP₄₃₅-R-PYP₃₆₀ (trace 1; after excitation at 355 nm), R-PYP₃₆₀-R-PYP₄₃₅ (trace 3; after subsequent excitation at 445 nm), and the baseline (trace 2; calculated as the sum of the two spectra). B, chromophore protonation and isomerization state: FT-IR difference spectra for pB₃₅₅-E-PYP₄₄₆ (trace 5), pB₃₆₀-R-PYP₄₄₆ (trace 4), and R-PYP₄₃₅-R-PYP₃₆₀ (trace 1). The indicated bands report about the chromophore protonation and isomerization state and the carboxylic group of Glu-46. The values for the band positions are taken from the literature (14, 27, 28).

intermediates. One of these species absorbing in the red (compared with the ground state pG₄₄₆) is similar to pR of E-PYP, with an absorption maximum at about 465 nm (pR₄₆₅). The major contribution to the spectrum of the first component is provided by a species with an absorption maximum around 415 nm (pB₄₁₅). The nature of this species is unclear. The only state of PYP with similar absorption characteristics reported so far is the low temperature state PYP_{BL} (32). A third contribution comes from a state with maximal absorption around 360 nm (pB'₃₆₀). In the next species-associated spectrum (after a couple of microseconds at 20 °C) the relative contribution of pB₄₁₅ has decreased, but on the other hand the contribution of pB'₃₆₀ has increased. Later on, this mixture of presumably three species is converted with a time constant of 17 μ s (20 °C) into a blue-shifted form with an absorption maximum at 360 nm (pB₃₆₀), similar to pB from E-PYP. pB₃₆₀ and pB'₃₆₀ have the same absorption spectra but may differ in their protein conformation. These two species might also be identical.

A model for the photocycle scheme of R-PYP is shown in Fig. 9. For R-PYP₄₄₆ (in analogy with E-PYP) the initial step after light absorption is the photoisomerization of the chromophore from *trans* to *cis*, leading to the formation of a red-shifted intermediate, pR₄₆₅. In addition, a species with a protonated chromophore ($\lambda_{\text{max}} = \sim 360$ nm), never detected so early in the photocycles of PYP(-like) proteins, and another intermediate

with so-far unknown characteristics (pB₄₁₅) are formed. Those three species exist in a mixture (indicated as X_1 and X_2 in Fig. 9), most probably in a thermal equilibrium (compare the different relative concentrations at 7 and 20 °C). The blue-shifted absorption spectra of pB₄₁₅ and pB'₃₆₀ point toward a (partly) protonated chromophore. Such a situation has been described earlier for the E-PYP mutant Y42F, where a species with absorption at 391 nm can be observed in the ground state of the protein (31), which is attributed to a not fully protonated chromophore. Later on in the photocycle the composition of the mixture, consisting of pR₄₆₅, pB₄₁₅, and pB'₃₆₀, is changing, and subsequently pB₃₆₀ is accumulated with a time constant of 17 μ s at 20 °C. pB₃₆₀ finally returns into the ground state R-PYP₄₄₆ with a time constant of 2.5 ms.

The FT-IR difference spectrum pB₃₆₀-R-PYP₄₄₆ supports the above stated model at several points. Looking on the marker bands for protonation and isomerization state it is clear that the chromophore in R-PYP₄₄₆ is deprotonated and in *trans* conformation, whereas in its photoproduct pB₃₆₀ it is protonated and in *cis* conformation (see Fig. 8 and Table II), a behavior similar to that found for E-PYP₄₄₆. Furthermore, during the photocycle as for E-PYP, Glu-46 becomes deprotonated (see below). It is likely that it acts as a proton donor for the chromophore during the photocycle of E-PYP, as well as of R-PYP₄₄₆. In R-PYP₄₄₆, the negative charge of the phenolic oxygen of the chromophore is stabilized by hydrogen bonding to Glu-46. The proton is less strongly bound to COO⁻ from Glu-46 compared with E-PYP₄₄₆ (downshift of 10 cm⁻¹). This could reflect a lower pK_a for Glu-46 in the (more) open chromophore pocket of R-PYP (see below) with respect to that of E-PYP.

The structure of the pB₃₆₀ form of R-PYP is most probably different from that of E-PYP, especially in its extent of conformational changes, which is supposedly lower in the case of R-PYP. Besides the kinetic argument (2.5- versus 400-ms lifetime for R-PYP and E-PYP, respectively) there is other support for this hypothesis. The role of methionine 100 has been extensively studied in E-PYP (34, 35). It has been suggested that Met-100 facilitates the conformational changes of the chromophore and/or the surrounding amino acids on the way back to the ground state (35). In all cases, replacement of the electron donating Met-100 by other amino acids slowed down the E-PYP recovery reaction significantly (by a factor of 20 to 2000). In R-PYP, Met-100 is replaced by a glycine, but the recovery kinetics are 100 times faster compared with wild-type E-PYP. This opposite finding in R-PYP (a much faster recovery) suggests that the protein conformation and/or the protein environment of the chromophore in R-PYP are probably different from that in E-PYP.

R-PYP₃₆₀ Photocycle—Besides the R-PYP₄₄₆ photocycle we also show the ability of R-PYP₃₆₀ to undergo a photocycle. After photoexcitation of R-PYP₃₆₀ a clear bleach in the absorption around 360 nm is observed. This bleach is accompanied by the accumulation of a red-shifted intermediate with an difference absorption maximum around 435 nm (R-PYP₄₃₅). During this process the chromophore undergoes a *cis* to *trans* isomerization and deprotonation (see also further below). The ground state R-PYP₃₆₀ is recovered via a slow thermal reisomerization and reprotonation in the dark. Recovery can be accelerated by a light-induced reisomerization using a subsequent blue flash (450 nm). Even though there are several examples of (E-)PYP variants described in the literature, which have two absorption maxima in the ground state (E-PYP mutants Y42F (31, 36), E46D, and E46A) (37), this is the first (well described) example of the occurrence of two independent photocycles in PYP.

The FT-IR difference spectrum R-PYP₃₆₀-R-PYP₄₃₅ contains a number of crucial information about the PYP chromophore.

TABLE II
Important infrared absorption bands (in cm^{-1}) for R-PYP₄₄₆, pB₃₆₀, R-PYP₃₆₀, R-PYP₄₃₅, E-PYP₄₄₆, and E-PYP₃₅₅

Assignment	Glu-46 (C=O) stretch	Deprotonated chromophore	Protonated chromophore	<i>trans</i> -isomer	<i>cis</i> -isomer
R-PYP ₄₄₆	1727	1489	— ^a	1303/1159	—
pB ₃₆₀	—	—	1513	—	1283/1175
R-PYP ₃₆₀	—	—	1516	—	1287/1170
R-PYP ₄₃₅	—	1488	—	1304/1158	—
E-PYP ₄₄₆	1736	1489	—	1302/1162	—
pB ₃₅₅	—	—	1511	—	1285/1174
Literature values (E-PYP) ^b	1737	1485	1515	1302/1163	1286/1175

^a Dash, Not observed.

^b From Refs. 14, 27, and 28.

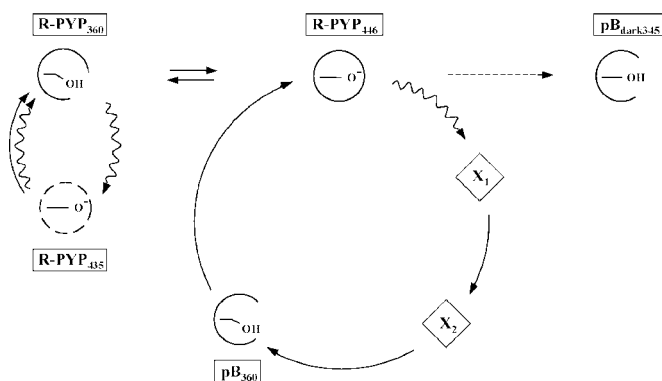


FIG. 9. Model of R-PYP including the ground state equilibrium between R-PYP₄₄₆ and R-PYP₃₆₀ and the two independent photocycles of both forms. Symbols indicate the isomerization and protonation state of the chromophore and the conformation of the protein. X₁ and X₂ represent a mixture of intermediates formed in the R-PYP₄₄₆ photocycle (for details see text).

The chromophore of R-PYP₃₆₀ is deprotonated and in *cis* configuration (see Fig. 8 and Table II). On the other hand, R-PYP₄₃₅ is protonated and in *trans* configuration. Surprisingly, Glu-46 does not change its protonation state. With respect to other parts of this study, it is likely to assume that Glu-46 is deprotonated, or at least not hydrogen-bonded to the chromophore, in R-PYP₃₆₀. This is a strong argument for a significant structural difference in R-PYP₃₆₀ compared with R-PYP₄₄₆ and E-PYP₄₄₆ with respect to the pK_a of Glu-46. Glu-46 behaves much more like a glutamic acid in solution. Because concomitantly the pK_a of the chromophore is upshifted by many orders of magnitudes compared with E-PYP₄₄₆ and R-PYP₄₄₆ it seems justified to propose that its solvent accessibility in R-PYP₃₆₀ is much larger compared with E-PYP₄₄₆ and R-PYP₄₄₆.

Despite differences in relative amplitudes, a number of pronounced infrared absorption bands have been found for R-PYP that are not present or weak for E-PYP. The most prominent are the bands at 1145 and 993 cm^{-1} . The latter might well be a hydrogen-out-of-plane mode reflecting a large strain for the chromophore in R-PYP₄₃₅. These bands indicate that the photocycle(s) of R-PYP are different, although similarities might be seen in the transient absorption changes.

Nile Red—To obtain information about the conformational state of both species of R-PYP we used the fluorescent hydrophobicity probe Nile Red (38). This probe was employed recently to examine conformational changes occurring during the photocycle of E-PYP (12). It was shown that NR binds to E-PYP upon formation of pB₃₅₅, when a hydrophobic region of the protein is exposed. No binding of NR to E-PYP in the ground state was observed. In contrast, addition of NR to ground state R-PYP leads to an increase and a strong blue shift in the fluorescence emission of NR, indicating binding of NR to an exposed hydrophobic surface. We attribute this finding to the

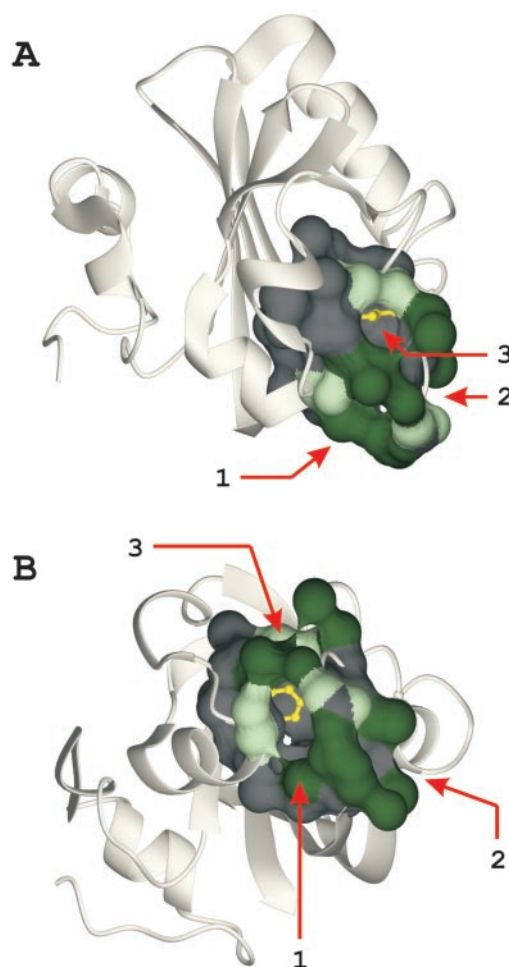


FIG. 10. 3D view of the chromophore binding pocket of R-PYP.

A backbone ribbon structure, with the chromophore binding pocket superposed, is shown in two views (A and B). The atoms forming the chromophore binding pocket were obtained via a CastP analysis (see text) of the modeled structure of R-PYP (39). The pocket is represented by a solvent contact surface (1.4-Å probe) with atoms lining the mouth openings in green and the other atoms in dark gray. The chromophore is shown as ball and stick in yellow. In panel A the chromophore can be observed through mouth opening 3. In panel B the view in panel A was rotated upward to show the chromophore through mouth opening 1 (the largest of the three). Mouth opening 2 opens up into the same tunnel to the chromophore as mouth opening 1. Light green atoms belong to Ile-66 (mouth 3), Ala-50 (mouth 1), and Gly-100 (shared by mouth 1 and 2). The figure was prepared using the program MOLMOL (33). The program POV-RayTM (www.povray.org) was used to render the images.

presence of R-PYP₃₆₀, because an increase in the relative concentration of R-PYP₃₆₀ at lower temperature leads to a further increase in NR binding. Moreover, results obtained with apo-R-PYP reconstituted with a *trans*-locked chromophore show almost no binding of NR. Note that the interaction of R-PYP₃₆₀ with NR is not identical with that of the signaling state pB₃₅₅

from E-PYP (12), indicated by the differences in the maximum of NR emission, 620 and 600 nm, respectively.

R-PYP₄₄₆ and R-PYP₃₆₀ are also part of a pH-dependent equilibrium. The pK_a of this transition was determined as 6.5 (18). The NR emission spectra after binding to R-PYP recorded at pH 8 and pH 5 differ in their characteristics. Besides the increase in the amplitude at pH 5, because of a higher concentration of R-PYP₃₆₀, the maximum of the emission has also changed. The red shift in emission can be attributed to a more polar environment for binding of NR, presumably caused by protonation of an amino acid near or in the NR binding pocket.

To determine possible NR binding sites, we subjected the model of the three-dimensional structure of R-PYP (39) to a search for structural pockets and cavities. Therefore we used the program CastP, which is publicly available (40) and which provides identification and measurements of surface-accessible pockets, as well as interior-inaccessible cavities, for proteins and other molecules. This analysis revealed the chromophore binding pocket as the largest pocket in R-PYP. More importantly, the results of the CastP analysis show that the chromophore binding pocket is not buried inside the protein, as is the case for E-PYP, but that it has direct access to the solvent. This contact is provided via three mouths, located around the amino acids Ile-66, Gly-100, and Ala-50 (numbering according to alignment with E-PYP; amino acids corresponding to Val-66, Met-100, and Thr-50 in E-PYP). The entries provided via Gly-100 and Ala-50 both lead into a large tunnel toward the chromophore (as shown in Fig. 10). This tunnel runs along the loop that connects strands 4 and 5 of the central β -sheet (5) and which forms the back side of the active site pocket in E-PYP. Met-100 and Thr-50 are key residues in the properties of E-PYP. Both residues shield the chromophore from the hydrophilic environment because of the presence of a rather large side chain and because of the establishment of a hydrogen bonding network with Arg-52 for Met-100 and with Tyr-42 and Arg-52 for Thr-50. Mutation of these amino acids lead to severe changes in the characteristics of E-PYP, which are reflected in the spectral properties and the photocycle kinetics (34, 41, 42). In R-PYP natural substitution of these amino acids to Ala-50 and Gly-100 makes the chromophore binding pocket accessible to the solvent and therefore is very likely responsible for the observed differences in the properties of both proteins (see below).

Model—A schematic model describing the different species and intermediates of R-PYP is depicted in Fig. 9. The two ground state forms of R-PYP characterized by their different absorption maxima (R-PYP₄₄₆ and R-PYP₃₆₀) are in a temperature- and pH-dependent equilibrium (18).

R-PYP₄₄₆ is characterized by the presence of a deprotonated *trans* chromophore (according to the FT-IR results presented in this paper and in analogy with E-PYP (3, 43, 44)). In contrast, R-PYP₃₆₀ has a different protein conformation with an increased accessible hydrophobic surface, as shown from the NR bindings studies. The chromophore of R-PYP₃₆₀ is protonated, as already indicated by the strong blue shift in the absorption maximum and confirmed by results from FT-IR spectroscopy. Additionally, we have shown by FT-IR spectroscopy that the chromophore in R-PYP₃₆₀ is in *cis* conformation. The latter conclusion is supported by the following. (i) Apo-R-PYP reconstituted with a *trans*-locked chromophore shows only a single peak in the absorption spectrum, corresponding to R-PYP₄₄₆; i.e. R-PYP₃₆₀ is absent (18). (ii) The different photocycles of R-PYP₄₄₆ and R-PYP₃₆₀ imply a different conformation of the chromophore in both species. In the photocycle of R-PYP₄₄₆ a blue-shifted intermediate (pB_{360}) is accumulated, characterized by a protonated *trans*- to *cis*-isomerized chromophore (in

analogy with E-PYP) (44). In contrast, the photoactivation of R-PYP₃₆₀ gives rise to the formation of a red-shifted intermediate (R-PYP₄₃₅), via *cis*- to *trans*-isomerization and deprotonation as indicated by our FT-IR analysis. R-PYP₄₃₅ can return to its ground state (R-PYP₃₆₀) (including a re-isomerization) either slowly in the dark or mediated by a 450-nm light flash.

The proposed features for R-PYP₄₄₆ and R-PYP₃₆₀ imply a temperature- and pH-dependent equilibrium, where lowering the temperature or pH induces a transition from R-PYP₄₄₆ to R-PYP₃₆₀ through changes in the protein conformation, as indicated by the Nile Red binding results, accompanied by dark isomerization and protonation of the chromophore. Increasing the temperature or pH triggers the opposite conversion. The pH dependence, with a pK_a of 6.5, can be explained by the presence of the large chromophore binding pocket that is accessible to the solvent, as also indicated by the CastP analysis. Changing the pH of the solvent will have a direct effect on the protonation state of one or more of the amino acids in the pocket. A possible candidate for this process is Glu-46, which has a proposed theoretical pK_a value of 6.4 in E-PYP (45). However, protonation of this amino acid would directly influence the protonation state of the chromophore and with that the spectral properties of the protein. A decrease of the pH below 4.5 leads to the formation of R-PYP₃₄₅ (analog to pB_{dark} from E-PYP) via unfolding of R-PYP₄₄₆ and protonation of the chromophore.

Acknowledgment—Robert Cordfunke is gratefully acknowledged for the preparation of protein samples.

REFERENCES

- Kort, R., Hoff, W. D., Van West, M., Kroon, A. R., Hoffer, S. M., Vlieg, K. H., Crielaand, W., Van Beeumen, J. J., and Hellingwerf, K. J. (1996) *EMBO J.* **15**, 3209–3218
- Meyer, T. E. (1985) *Biochim. Biophys. Acta* **806**, 175–183
- Hoff, W. D., Dux, P., Hard, K., Devreese, B., Nugteren-Roodzant, I. M., Crielaand, W., Boelens, R., Kaptein, R., Van Beeumen, J., and Hellingwerf, K. J. (1994) *Biochemistry* **33**, 13959–13962
- Baca, M., Borgstahl, G. E., Boissinot, M., Burke, P. M., Williams, D. R., Slater, K. A., and Getzoff, E. D. (1994) *Biochemistry* **33**, 14369–14377
- Borgstahl, G. E., Williams, D. R., and Getzoff, E. D. (1995) *Biochemistry* **34**, 6278–6287
- Pellequer, J. L., Wager-Smith, K. A., Kay, S. A., and Getzoff, E. D. (1998) *Proc. Natl. Acad. Sci. U. S. A.* **95**, 5884–5890
- Taylor, B. L., and Zhulin, I. B. (1999) *Microbiol. Mol. Biol. Rev.* **63**, 479–506
- Uij, L., Devanathan, S., Meyer, T. E., Cusanovich, M. A., Tollin, G., and Atkinson, G. H. (1998) *Biophys. J.* **75**, 406–412
- Gensch, T., Gradinaru, C., van Stokkum, I., Hendriks, J., Hellingwerf, K., and van Grondelle, R. (2002) *Chem. Phys. Lett.* **356**, 347–354
- Meyer, T. E., Yakali, E., Cusanovich, M. A., and Tollin, G. (1987) *Biochemistry* **26**, 418–423
- Hoff, W. D., van Stokkum, I. H., van Ramesdonk, H. J., van Brederode, M. E., Brouwer, A. M., Fitch, J. C., Meyer, T. E., van Grondelle, R., and Hellingwerf, K. J. (1994) *Biophys. J.* **67**, 1691–1705
- Hendriks, J., Gensch, T., Hvuid, L., van Der Horst, M. A., Hellingwerf, K. J., and van Thor, J. J. (2002) *Biophys. J.* **82**, 1632–1643
- Xie, A., Kelemen, L., Hendriks, J., White, B. J., Hellingwerf, K. J., and Hoff, W. D. (2001) *Biochemistry* **40**, 1510–1517
- Genick, U. K., Devanathan, S., Meyer, T. E., Canestrelli, I. L., Williams, E., Cusanovich, M. A., Tollin, G., and Getzoff, E. D. (1997) *Biochemistry* **36**, 8–14
- Van Brederode, M. E., Hoff, W. D., Van Stokkum, I. H., Groot, M. L., and Hellingwerf, K. J. (1996) *Biophys. J.* **71**, 365–380
- Meyer, T. E., Fitch, J. C., Bartsch, R. G., Tollin, G., and Cusanovich, M. A. (1990) *Biochim. Biophys. Acta* **1016**, 364–370
- Jiang, Z., Swem, L. R., Rushing, B. G., Devanathan, S., Tollin, G., and Bauer, C. E. (1999) *Science* **285**, 406–409
- Haker, A., Hendriks, J., Gensch, T., Hellingwerf, K. J., and Crielaand, W. (2000) *FEBS Lett.* **486**, 52–56
- Hoff, W. D., Van Stokkum, I. H. M., Gural, J., and Hellingwerf, K. J. (1997) *Biochim. Biophys. Acta* **1322**, 151–162
- Cordfunke, R., Kort, R., Pierik, A., Gobets, B., Koomen, G. J., Verhoeven, J. W., and Hellingwerf, K. J. (1998) *Proc. Natl. Acad. Sci. U. S. A.* **95**, 7396–7401
- Hendriks, J., van Stokkum, I. H., Crielaand, W., and Hellingwerf, K. J. (1999) *FEBS Lett.* **458**, 252–256
- van Stokkum, I. H. M., and Lozier, R. H. (2002) *J. Phys. Chem. B* **106**, 3477–3485
- van Stokkum, I., Scherer, T., Brouwer, A., and Verhoeven, J. (1994) *J. Phys. Chem.* **98**, 852
- Kroon, A. R., Hoff, W. D., Fennema, H. P., Gijzen, J., Koomen, G. J., Verhoeven, J. W., Crielaand, W., and Hellingwerf, K. J. (1996) *J. Biol. Chem.* **271**, 31949–31956

25. Heberle, J., and Zscherp, C. (1996) *Appl. Spectrosc.* **50**, 588–596
26. Nyquist, R., Heitbrink, D., Bolwien, C., Wells, T., Gennis, R. B., and Heberle, J. (2001) *FEBS Lett.* **505**, 63–67
27. Brudler, R., Rammelsberg, R., Woo, T. T., Getzoff, E. D., and Gerwert, K. (2001) *Nat. Struct. Biol.* **8**, 265–270
28. Imamoto, Y., Shirahige, Y., Tokunaga, F., Kinoshita, T., Yoshihara, K., and Kataoka, M. (2001) *Biochemistry* **40**, 8997–9004
29. Hoff, W. D., Xie, A., Van Stokkum, I. H., Tang, X. J., Gural, J., Kroon, A. R., and Hellingwerf, K. J. (1999) *Biochemistry* **38**, 1009–1017
30. Xie, A., Hoff, W. D., Kroon, A. R., and Hellingwerf, K. J. (1996) *Biochemistry* **35**, 14671–14678
31. Brudler, R., Meyer, T. E., Genick, U. K., Devanathan, S., Woo, T. T., Millar, D. P., Gerwert, K., Cusanovich, M. A., Tollin, G., and Getzoff, E. D. (2000) *Biochemistry* **39**, 13478–13486
32. Imamoto, Y., Kataoka, M., and Tokunaga, F. (1996) *Biochemistry* **35**, 14047–14053
33. Koradi, R., Billeter, M., and Wuthrich, K. (1996) *J. Mol. Graph.* **14**, 51–55
34. Mataga, N., Chosrowjan, H., Shibata, Y., Imamoto, Y., and Tokunaga, F. (2000) *J. Phys. Chem. B* **104**, 5191–5199
35. Kumauchi, M., Hamada, N., Sasaki, J., and Tokunaga, F. (2002) *J. Biochem. (Tokyo)* **132**, 205–210
36. Mihara, K., Hisatomi, O., Imamoto, Y., Kataoka, M., and Tokunaga, F. (1997) *J. Biochem. (Tokyo)* **121**, 876–880
37. Devanathan, S., Brudler, R., Hessling, B., Woo, T. T., Gerwert, K., Getzoff, E. D., Cusanovich, M. A., and Tollin, G. (1999) *Biochemistry* **38**, 13766–13772
38. Sackett, D. L., and Wolff, J. (1987) *Anal. Biochem.* **167**, 228–234
39. Kort, R., Phillips-Jones, M. K., van Aalten, D. M., Haker, A., Hoffer, S. M., Hellingwerf, K. J., and Crielgaard, W. (1998) *Biochim. Biophys. Acta* **1385**, 1–6
40. Liang, J., Edelsbrunner, H., and Woodward, C. (1998) *Protein Sci.* **7**, 1884–1897
41. Devanathan, S., Genick, U. K., Canestrelli, I. L., Meyer, T. E., Cusanovich, M. A., Getzoff, E. D., and Tollin, G. (1998) *Biochemistry* **37**, 11563–11568
42. Sasaki, J., Kumauchi, M., Hamada, N., Oka, T., and Tokunaga, F. (2002) *Biochemistry* **41**, 1915–1922
43. Kim, M., Mathies, R. A., Hoff, W. D., and Hellingwerf, K. J. (1995) *Biochemistry* **34**, 12669–12672
44. Kort, R., Vonk, H., Xu, X., Hoff, W. D., Crielgaard, W., and Hellingwerf, K. J. (1996) *FEBS Lett.* **382**, 73–78
45. Demchuk, E., Genick, U. K., Woo, T. T., Getzoff, E. D., and Bashford, D. (2000) *Biochemistry* **39**, 1100–1113